CHAOS
Theory and Applications
in Applied Sciences and Engineering

e-ISSN: 2687-4539
RESEARCH ARTICLE
Vol.7 / No.1 / 2025 / pp.87-98
https://doi.org/10.51537/chaos.1581247

Bifurcation Analysis and Chaos Control of a Discrete-Time Fractional Order Predator-Prey Model with Holling Type II Functional Response and Harvesting

Agus Suryanto *,1, **Isnani Darti** *,2 **and Edi Cahyono** α,3

*Department of Mathematics, Faculty of Mathematics and Natural Sciences, University of Brawijaya, Malang-65145, Indonesia, αDepartment of Mathematics, Faculty of Mathematics and Natural Sciences, Halu Oleo University, Kendari-93232, Indonesia.

ABSTRACT This paper employs a piecewise constant approximation to discretize a fractional order Holling type II predator-prey model with harvesting in both populations. The dynamics of the resulting discrete-time model are then investigated. First, the conditions for fixed points' existence and stability are established. It is also demonstrated that the proposed discrete-time model can undergo either flip bifurcation or Neimark-Sacker bifurcation. The existence and direction of both bifurcations have been identified using the center manifold theorem. The appearance of these bifurcations results in the emergence of chaotic dynamics. To stabilize chaos at the fixed point of unstable trajectories, we provide two types of control chaos: hybrid control and state feedback control. By selecting appropriate control settings, it is shown that both hybrid control and state feedback control eliminate chaotic orbits and make the fixed point asymptotically stable. Some numerical simulations were used to verify all analytical conclusions.

KEYWORDS
Discrete-time model
Fractional order
Flip bifurcation
Neimark-Sacker bifurcation
Chaos control

INTRODUCTION

Predator-prey interaction is regarded as an essential component of the food chain, making it one of the most extensively researched concerns in ecology and mathematical biology (Brown *et al.* 2004). Predator-prey interactions are investigated to get better understanding on their population dynamics and predict possible extinctions (Berryman 1992; Beretta and Kuang 1998). The study of predator-prey systems is not only beneficial in developing scientific theories, but it is also crucial to the establishment of a sustained human society as well as environmental health (Guo *et al.* 2023).

Many scholars have recommended significant changes to the system by incorporating ecological aspects such as functional responses (Holling 1965), Allee effect (Panigoro *et al.* 2023; Sahoo and Sahoo 2024; Mandal *et al.* 2025), additional food (Ulfa *et al.* 2017; Mondal *et al.* 2024), cannibalism (Rayungsari *et al.* 2022; Shabbir and Din 2022), harvesting (Suryanto *et al.* 2019; Guo *et al.* 2023; Panigoro *et al.* 2023; Sarkar and Mondal 2023), and more. The functional response in predator-prey interaction is a significant factor because it specifies the amount of prey consumed per predator per unit time, given the available prey (Uddin *et al.* 2024; Sarkar and Mondal 2023). Holling developed three sorts of functional responses to describe mathematically predators' prey consumption: Holling types I, II, and III (Holling 1965, 1966). The Holling type I functional response is appropriate for situations where predators have access to a large population of prey. Holling types II and III are monotonic and exhibit a saturation effect when prey population is large. In particular, the Holling type II functional response reflects a reduction in intake levels due to limited prey. This functional response involves two key parameters: handling time and attack rate. The Holling type II functional response has been frequently used in predator-prey models, as shown in (Mukhopadhyay and Bhattacharyya 2016; Zhang *et al.* 2019).

Manuscript received: 7 November 2024,
Revised: 22 February 2025,
Accepted: 16 March 2025.

[1]suryanto@ub.ac.id (**Corresponding author**)
[2]isnanidarti@ub.ac.id
[3]edi.cahyono@uho.ac.id

Harvesting of one or both species in a predator-prey system is another critical aspect in predator-prey dynamics. Harvesting ecological resources is typically done as part of integrated agriculture pest management, fisheries, forestry, and wildlife management programs. Because of the long-term benefits to people, bio-economic models have been developed for scientific management of renewable resources. Lee and Baek (2017) examined a predator-prey model with a constant harvest rate. The research team investigated the predator-prey model, which included linear harvesting of prey and predators. Mukhopadhyay and Bhattacharyya (2016) examined a model with two predators fighting for the same prey and investigated the implications of harvesting.

The predator-prey interaction models described above are expressed as first-order differential equations. In these models, the population growth rate is only determined instantaneously. Numerous researchers have recommended employing fractional order derivatives to account for memory effects. For example, Hasan *et al.* (2022) offered a fractional order Leslie-Gower model that includes Allee effect and prey refuge. Rayungsari *et al.* (2023) investigated a fractional order predator-prey model that takes into account the impacts of cannibalism and predator refuge. We have also developed a number of fractional order predator-prey models in the presence of pathogen infection, including (Panigoro *et al.* 2019, 2021).

Recently, Sarkar and Mondal (2023) introduced a fractional order predator-prey model with linear harvesting for both prey and predator population, namely

$$\begin{aligned} D^{\alpha}\hat{x} &= r\hat{x}(1-\frac{\hat{x}}{K}) - \frac{\sigma\hat{x}\hat{y}}{1+m\hat{x}} - k_1\hat{x} \\ D^{\alpha}\hat{y} &= \frac{\beta\hat{x}\hat{y}}{1+m\hat{x}} - f\hat{y} - k_2\hat{y}, \end{aligned} \tag{1}$$

where $\hat{x} = \hat{x}(\tau)$ and $\hat{y} = \hat{y}(\tau)$ denote the prey and predator population at time τ. In this case, r, K, σ, β, m, and f are positive-valued parameters which respectively indicate the intrinsic growth rate of prey, the environmental carrying capacity of prey, the rate of predation, the conversion rate of predation, the handling time to catch and devour the prey population, and the natural death rate of predators. k_1 and k_2 are respectively the harvesting rate of prey and predator. D^{α} represents the Caputo fractional derivative of order α where $\alpha \in (0,1]$, which is defined as (Petráš 2011)

$$D^{\alpha}u(\tau) = \frac{1}{\Gamma(1-\alpha)}\int_0^{\tau}\frac{u'(s)}{(\tau-s)^{\alpha}}\,ds. \tag{2}$$

To simplify the analysis, we introduce the following transformation

$$\hat{x} = Kx, \;\; \hat{y} = \frac{rmK}{\sigma}y, \;\; \text{and} \;\; \tau = t/r,$$

such that model (1) can be written as

$$\begin{aligned} D^{\alpha}x &= x(1-x) - \frac{xy}{a+x} - px \\ D^{\alpha}y &= \frac{bxy}{a+x} - (c+q)x, \end{aligned} \tag{3}$$

where

$$a = \frac{1}{mK}, \;\; b = \frac{\beta}{rm}, \;\; p = \frac{k_1}{r}, \;\; c = \frac{f}{r}, \text{and} \;\; q = \frac{g}{r}.$$

While fractional order models can represent memory effects in predator-prey interactions, numerous scholars choose to explore discrete-time models. Discrete models are thought to be better suited for explaining many phenomena in biology and have more complex dynamics than continuous ones (Santra and Mahapatra 2020; Alzabut *et al.* 2022; Panigoro *et al.* 2023). One method for obtaining a discrete–time model is to discretize the continuous one. For example, a discrete–time version of the first order predator–prey model with Holling type II without harvesting has been studied by Khan *et al.* (2019); Liu and Li (2021); Arias *et al.* (2022). In this case, Liu and Li (2021) applied a semidiscretization method, while Khan *et al.* (2019) implemented a nonstandard finite difference scheme. In order to solve a system of fractional order ordinary differential equations (FODE), El-Sayed and Salman (2013) proposed the piecewise constant approximation (PWCA) method. Following that, several scholars adapted the PWCA method for a variety of biological mechanisms. Selvam *et al.* (2020) and Mondal *et al.* (2020) have independently implemented the PWCA approach for a fractional order predator-prey model with Holling type II functional response and prey refuge, but no harvesting. Al-Nassir (2021) has investigated a discrete model for fractional order predator-prey model with harvesting obtained from the PWCA approach, although the functional response is Holling type III. In this study, we consider a discrete-time version of model (3), which is derived using the PWCA approach. We recognize that the PWCA approach relies on the fact that the exact solution of a FODE

$$D^{\alpha}u(t) = f(t,u(t)), \;\; u(0) = u_0, \tag{4}$$

can be written as

$$u(t) = u(0) + \frac{1}{\Gamma(\alpha)}\int_0^t (t-\tau)^{\alpha-1}f(\tau,u(\tau))d\tau. \tag{5}$$

If the function $f(t,u(\tau))$ is assumed to be constant for $\tau \in [0,t)$, i.e., $f(t,u(\tau)) = \bar{f}$, then the solution (5) leads to

$$\begin{aligned} u(t) &= u(0) + \frac{1}{\Gamma(\alpha)}\int_0^t (t-\tau)^{\alpha-1}f(\tau,u(\tau))d\tau \\ &= u(0) + \frac{\bar{f}}{\Gamma(\alpha)}\int_0^t (t-\tau)^{\alpha-1}d\tau \\ &= u(0) + \frac{\bar{f}t^{\alpha}}{\Gamma(\alpha)}. \end{aligned} \tag{6}$$

To discretize system (3), we suppose that the time domain is divided into a finite number of sub-intervals $t_{m-1} < t < t_m, m = 1,2,\ldots,N$. The solution is determined by applying equation (5) and assuming that the solution is constant in each sub-interval, namely $u(t) = u_{m-1} = u(t_{m-1})$ for $t \in [t_{m-1}, t_m)$. In this way, we obtain a PWCA scheme for model (3) as follows

$$\begin{aligned} x_{n+1} &= x_n + \delta\left[(1-x_n)x_n - \frac{x_n y_n}{a+x_n} - px_n\right] \\ y_{n+1} &= y_n + \delta\left[\frac{bx_n y_n}{a+x_n} - (c+q)y_n\right], \end{aligned} \tag{7}$$

where $\delta = \frac{h^{\alpha}}{\alpha\Gamma(\alpha)}$ and h is the time step size of numerical integration. Notice that when the order of fractional derivative is $\alpha = 1$ then scheme (7) is the forward Euler scheme for the model (3).

This work examines the dynamics of the discrete-time model (7). To accomplish this, we first study the existence and stability of all possible fixed points, then proceed to bifurcation analysis (flip and Neimark-Sacker bifurcations). We may predict the occurrence of chaos in our discrete system, just as we have in other discrete systems. As consequently, we provide two distinct types of chaos control: hybrid control and state feedback control. The hybrid control has been successfully applied by Panigoro *et al.* (2023) and Ruan and Li (2024) to eliminate the occurrence of the chaotic

solution. The effective implementation of the state feedback control to prevent chaotic behavior has been demonstrated (Ruan and Li 2024; Khan *et al.* 2024; Li *et al.* 2024). Finally, numerical simulations are used to validate and elucidate the theoretical results.

FIXED POINTS AND THEIR STABILITY PROPERTIES

Existence of Fixed Points

The fixed points of the discrete system (7) can be determined by solving the following system of algebraic equations

$$\begin{aligned} x &= x + \delta\left[1 - x - \frac{y}{a+x} - p\right]x \\ y &= y + \delta\left[\frac{bx}{a+x} - (c+q)\right]y. \end{aligned} \tag{8}$$

It can be shown that system (7) has three fixed points, that are

$$E_0 = (0,0), \qquad E_1 = (1-p,0), \qquad E^* = (x^*, y^*) \tag{9}$$

where

$$x^* = \frac{a(c+q)}{b-(c+q)}, \text{ and } y^* = \frac{ab((1-p)(b-(c+q)) - a(c+q))}{(b-(c+q))^2}.$$

It is clear that the extinction of both population fixed point (E_0) always exists. Furthermore, the extinction of predator fixed point (E_1) exists if $p < 1$, while the interior fixed-point E^* exists if all following conditions are satisfied

1. $p < 1$,
2. $b > c + q$, and
3. $(1-p) > \frac{a(c+q)}{b-(c+q)}$.

Stability of Fixed Points

In this part we study the stability properties of all fixed-points by observing system (7) around each fixed point. The Jacobian matrix of system (7) evaluated at a fixed point $\bar{E} = (\bar{x}, \bar{y})$ is

$$J(E(\bar{x},\bar{y})) = \begin{bmatrix} 1 + \delta\left[1 - 2\bar{x} - p - \frac{a\bar{y}}{(a+\bar{x})^2}\right] & -\delta\left[\frac{\bar{x}}{a+\bar{x}}\right] \\ \delta\left[\frac{ab\bar{y}}{(a+\bar{x})^2}\right] & 1 + \delta\left[\frac{b\bar{x}}{(a+\bar{x})} - (c+q)\right] \end{bmatrix}. \tag{10}$$

If λ_1 and λ_2 are eigenvalues of the Jacobian matrix (10), then the fixed point $\bar{E}$ is asymptotically stable if $|\lambda_{1,2}| < 1$. If $|\lambda_1| = 1$ or $|\lambda_2| = 1$, then $\bar{E}$ is a non-hyperbolic fixed point. We now investigate the stability properties of each fixed point.

It is easy to check that the Jacobian matrix at $E_0 = (0,0)$ is

$$J(E_0) = \begin{bmatrix} 1 + \delta(1-p) & 0 \\ 0 & 1 - \delta(c+q) \end{bmatrix}, \tag{11}$$

where its eigenvalues are

$$\lambda_1 = 1 + \delta(1-p), \qquad \lambda_2 = 1 - \delta(c+q).$$

It is directly observed that $\lambda_1 > 1$ if $p < 1$. For $p > 1$, $|\lambda_1| < 1$ if and only if $\delta < \frac{2}{p-1} \Leftrightarrow h < \sqrt[\alpha]{\frac{2\alpha\Gamma(\alpha)}{p-1}} = h_1$. Similarly, we have that $|\lambda_2| < 1 \Leftrightarrow \delta < \frac{2}{c+q} \Leftrightarrow h < \sqrt[\alpha]{\frac{2\alpha\Gamma(\alpha)}{c+q}} = h_2$. By observing those eigenvalues using the same method, we can prove the following results. The fixed point E_0 is

1. a sink if $p > 1$ and $0 < h < \min\{h_1, h_2\}$.
2. a source if one of the following conditions holds
   (a) $p < 1$ and $h > h_2$,
   (b) $p > 1$ and $h > \max\{h_1, h_2\}$.
3. a saddle if one of the following conditions holds
   (a) $p < 1$ and $0 < h < h_2$,
   (b) $p > 1$ and $\min\{h_1, h_2\} < h < \max\{h_1, h_2\}$.
4. a non-hyperbolic if one of the following conditions holds
   (a) $p = 1$,
   (b) $p > 1$ and $h = h_1$,
   (c) $h = h_2$.

If the fixed point $E_1 = (1-p, 0)$ is substituted into the Jacobian matrix (10), then we obtain

$$J(E_1) = \begin{bmatrix} 1 - \delta(1-p) & -\frac{\delta(1-p)}{a+(1-p)} \\ 0 & 1 + \delta\left(\frac{b(1-p)}{a+(1-p)} - (c+q)\right) \end{bmatrix}. \tag{12}$$

The eigenvalues of the Jacobian matrix $J(E_1)$ are

$$\lambda_1 = 1 - \delta(1-p), \qquad \lambda_2 = 1 + \delta\left(\frac{b(1-p)}{a+(1-p)} - (c+q)\right).$$

If E_1 exists, i.e. when $p < 1$, then $\lambda_1 < 1$. We also observe that if $(1-p) > L^*$ where $L^* = \frac{a(c+q)}{b-(c+q)}$ then $\lambda_2 > 1$. By evaluating the values of λ_1 and λ_2 in similar way, we conclude the following results regarding the topology of the fixed point E_1.

Let $h_3 = \sqrt[\alpha]{\frac{2\alpha\Gamma(\alpha)}{1-p}}$ and $h_4 = \sqrt[\alpha]{\frac{2\alpha\Gamma(\alpha)(a+(1-p))}{(a+(1-p))(c+q)-b(1-p)}}$. Then, the fixed point E_1 is

1. a sink if $(1-p) < L^*$ and $h < \min\{h_3, h_4\}$.
2. a source if one of the following conditions holds
   (a) $1 - p > L^*$ and $h > h_3$,
   (b) $1 - p < L^*$ and $h > \max\{h_3, h_4\}$.
3. a saddle if one of the following conditions holds
   (a) $1 - p > L^*$ and $0 < h < h_3$,
   (b) $1 - p < L^*$ and $\min\{h_3, h_4\} < h < \max\{h_3, h_4\}$.
4. a non-hyperbolic if one of the following conditions holds
   (a) $1 - p = L^*$,
   (b) $1 - p < L^*$ and $h = h_4$,
   (c) $h = h_3$.

The Jacobian matrix (10) evaluated at $E^* := (x^*, y^*)$ is

$$J(E^*) = \begin{bmatrix} 1 + \delta j_{11} & \delta j_{12} \\ \delta j_{21} & 1 \end{bmatrix}, \tag{13}$$

where

$$j_{11} = \frac{(c+q)}{b(b-(c+q))}((1-p)(b-(c+q)) - a(b+c+q)),$$
$$j_{12} = -\frac{c+q}{b} < 0,$$
$$j_{21} = (1-p)(b-(c+q)) - a(c+q).$$

The characteristics equation of the Jacobian matrix $J(E^*)$ is given by

$$F(\lambda) = \lambda^2 - Tr(J(E^*))\lambda + Det(J(E^*)) = 0 \tag{14}$$

where

$$Tr(J(E^*)) = 2 + \Psi_1\delta,$$
$$Det(J(E^*)) = 1 + \Psi_1\delta + \Psi_2\delta^2,$$

and

$$\Psi_1 = j_{11} = \frac{(c+q)}{b(b-(c+q))}((1-p)(b-(c+q)) - a(b+c+q)),$$
$$\Psi_2 = -j_{12}j_{21} = \frac{(c+q)}{b}\left((1-p)(b-(c+q)) - a(c+q)\right).$$

According to Liu and Xiao (2007), if λ_1 and λ_2 are characteristics roots of (14) and if $F(1) > 0$, then the following results hold.

1. $|\lambda_1| < 1$ and $|\lambda_2| < 1$ if and only if $F(-1) > 0$ and $Det(J(E^*)) < 1$.
2. $|\lambda_1| < 1$ and $|\lambda_2| > 1$ or $|\lambda_1| > 1$ and $|\lambda_2| < 1$ if and only if $F(-1) < 0$.
3. $|\lambda_1| > 1$ and $|\lambda_2| > 1$ if and only if $F(-1) > 0$ and $Det(J(E^*)) > 1$.
4. $\lambda_1 = -1$ and $|\lambda_2| \neq 1$ if and only if$F(-1) = 0$ and $Tr(J(E^*)) \neq 0, 2$.
5. λ_1 and λ_2 are a pair of conjugate complex roots with $|\lambda_1| = |\lambda_2| = 1$ if and only if $Tr(J(E^*))^2 - 4Det(J(E^*)) < 0$ and $Det(J(E^*)) = 1$.

From the characteristics equation (14), we can show that

1. $F(0) = 1 + \Psi_1\delta + \Psi_2\delta^2$,
2. $F(1) = \Psi_2\delta^2$,
3. $F(-1) = 4 + 2\Psi_1\delta + \Psi_2\delta^2$.

It is seen that if E^* exists then $j_{21} > 0$ and therefore $\Psi_2 > 0$. Consequently, $F(1) > 0$ and we can apply the above rules to evaluate the properties of λ_1 and λ_2. By analysing the values of $F(0) = Det(J(E^*))$ and $F(-1)$, and then implementing those above rules, the fixed point E^* has the following properties. Let $\Delta = \Psi_1^2 - 4\Psi_2$ and

$$\hat{\delta_0} = -\Psi_1/\Psi_2, \quad \hat{\delta_1} = \frac{-\Psi_1 - \sqrt{\Delta}}{\Psi_2}, \quad \hat{\delta_2} = \frac{-\Psi_1 + \sqrt{\Delta}}{\Psi_2}.$$

If E^* exists and $1 - p < L^* + \frac{ab}{b-(c+q)}$, then E^* is:

1. a sink if one of the following conditions holds
   (a) $\Delta < 0$ and $0 < h < \hat{h_0}$, where $\hat{h_0} = \sqrt[\alpha]{\alpha\Gamma(\alpha)\hat{\delta_0}}$,
   (b) $\Delta \geq 0$ and $0 < h < \hat{h_1}$, where $\hat{h_1} = \sqrt[\alpha]{\alpha\Gamma(\alpha)\hat{\delta_1}}$;
2. a source if one of the following conditions holds
   (a) $\Delta > 0$ and $h > \hat{h_2}$, where $\hat{h_2} = \sqrt[\alpha]{\alpha\Gamma(\alpha)\hat{\delta_2}}$,
   (b) $\Delta \leq 0$ and $h > \hat{h_0}$;
3. a saddle if $\Delta > 0$ and $\hat{h_1} < h < \hat{h_2}$;
4. a non-hyperbolic if one of the following conditions holds
   (a) $\Delta > 0$, $h = \hat{h_1}$, and $Tr(J(E^*)) = 2 + \Psi_1\delta \neq 0, -2$,
   (b) $\Delta > 0$, $h = \hat{h_2}$, and $Tr(J(E^*)) = 2 + \Psi_1\delta \neq 0, -2$,
   (c) $\Delta < 0$ and $h = \hat{h_0}$.

BIFURCATION ANALYSIS

This section examines the flip and Neimark-Sacker (NS) bifurcations at the fixed point $E^* = (x^*, y^*)$ of the model (7), utilizing the parameter h as a bifurcation parameter. Since $h = \sqrt[\alpha]{\alpha\Gamma(\alpha)\delta}$, δ can also be viewed as the bifurcation parameter. In this part, we also assume that $1 - p < L^* + \frac{ab}{b-(c+q)}$ and the order of fractional derivative is $\alpha \in (0, 1)$.

Flip Bifurcation

We first define a set of parameter $\Omega_j = \left\{(a, b, c, p, q, \delta, \alpha) \mid \Delta > 0, \delta = \hat{\delta_j},\ 2 + \Psi_1\delta \neq 0, -2;\right\}, j = 1, 2$. Remark that $\delta = \hat{\delta_j} \Leftrightarrow h = \hat{h_j}, j = 1, 2$. Based on the previous analysis, the Jacobian matrix $J(E^*)$ with $(a, b, c, p, q, \delta, \alpha) \in \Omega_j, j = 1, 2$ has eigenvalues $\lambda_1 = -1$ and $\lambda_2 \neq \pm 1$; indicating that a flip (period-doubling) bifurcation may occur from the fixed point E^* whenever $(a, b, c, p, q, \delta, \alpha)$ crosses region $\Omega_j, j = 1, 2$. Here we perform a flip bifurcation analysis around Ω_1. The flip bifurcation around Ω_2 can be analyzed analogously and is thus omitted. The flip bifurcation analysis is started by introducing a small perturbation $\bar{\delta}$, $|\bar{\delta}| \ll 1$ around $\delta = \hat{\delta_1}$ such that model (7) becomes

$$\begin{aligned} x_{n+1} &= x_n + (\hat{\delta_1} + \bar{\delta})\left[(1 - x_n)x_n - \frac{x_n y_n}{a + x_n} - px_n\right] \\ y_{n+1} &= y_n + (\hat{\delta_1} + \bar{\delta})\left[\frac{bx_n y_n}{a + x_n} - (c + q)y_n\right]. \end{aligned} \tag{15}$$

We translate the fixed point $E^* = (x^*, y^*)$ into the origin by using $u_n = x_n - x^*$ and $v_n = y_n - y^*$. The resulting system leads to, after Taylor expansion,

$$\begin{bmatrix} u_{n+1} \\ v_{n+1} \end{bmatrix} = \begin{bmatrix} a_{11} & a_{12} \\ a_{21} & a_{22} \end{bmatrix} \begin{bmatrix} u_n \\ v_n \end{bmatrix} + \begin{bmatrix} f_1(u_n, v_n, \bar{\delta}) \\ f_2(u_n, v_n, \bar{\delta}) \end{bmatrix} \tag{16}$$

where

$$\begin{aligned} f_1(u_n, v_n, \bar{\delta}) =& a_{13}u_n^2 + a_{14}u_n v_n + a_{15}v_n^3 + a_{16}u_n^2 v_n \\ &+ (b_1 u_n + b_2 v_n + b_3 u_n^2 + b_4 v_n^2)\bar{\delta} \\ f_2(u_n, v_n, \bar{\delta}) =& a_{23}u_n^2 + a_{24}u_n v_n + a_{25}v_n^3 + a_{26}u_n^2 v_n \\ &+ (c_1 u_n + c_2 v_n + c_3 u_n^2 + c_4 v_n^2)\bar{\delta} \end{aligned}$$

with

$$a_{11} = 1 + \hat{\delta_1}((1-x^*-p)\tfrac{c+q}{b} - x^*) \qquad b_1 = (1-x^*-p)\tfrac{c+q}{b} - x^*$$
$$a_{12} = -\tfrac{\hat{\delta_1}x^*}{a+x^*} \qquad b_2 = -\tfrac{x^*}{a+x^*}$$
$$a_{13} = \hat{\delta_1}\left(\tfrac{y^*}{(a+x^*)^2}(1-\tfrac{x^*}{a+x^*}) - 1\right) \qquad b_3 = \tfrac{y^*}{(a+x^*)^2}(1-\tfrac{x^*}{a+x^*}) - 1$$
$$a_{14} = -\tfrac{b-(c+q)}{b(a+x^*)}\hat{\delta_1} \qquad b_4 = -\tfrac{b-(c+q)}{b(a+x^*)}$$
$$a_{15} = -\tfrac{\hat{\delta_1}y^*}{(a+x^*)^3} \qquad a_{16} = \tfrac{\hat{\delta_1}}{(a+x^*)^2}(1-\tfrac{x^*}{a+x^*})$$
$$a_{21} = \tfrac{by^*\hat{\delta_1}}{a+x^*}(1-\tfrac{x^*}{a+x^*}) \qquad c_1 = \tfrac{by^*}{a+x^*}(1-\tfrac{x^*}{a+x^*})$$
$$a_{22} = 1 \qquad c_2 = 0$$
$$a_{23} = -\tfrac{by^*\hat{\delta_1}}{(a+x^*)^2}(1-\tfrac{x^*}{a+x^*}) \qquad c_3 = -\tfrac{by^*}{(a+x^*)^2}(1-\tfrac{x^*}{a+x^*})$$
$$a_{24} = \tfrac{b\hat{\delta_1}}{a+x^*}(1-\tfrac{x^*}{a+x^*}) \qquad c_4 = \tfrac{b}{a+x^*}(1-\tfrac{x^*}{a+x^*})$$
$$a_{25} = \tfrac{y^*\hat{\delta_1}}{(a+x^*)^3} \qquad a_{26} = \tfrac{b\hat{\delta_1}}{(a+x^*)^2}(\tfrac{x^*}{a+x^*} - 1).$$

The eigenvalues of the linearized system of (16) are $\lambda_1 = -1$ and $\lambda_2 = 3 + \Psi_1\hat{\delta_1}$. λ_2 is neither -1 nor 1 if $\hat{\delta_1} \neq -2/\Psi_1$ or $\hat{\delta_1} \neq -4/\Psi_1$. By taking

$$\begin{bmatrix} u_n \\ v_n \end{bmatrix} = \begin{bmatrix} a_{12} & a_{12} \\ -1-a_{11} & \lambda_2 - a_{11} \end{bmatrix} \begin{bmatrix} M_n \\ N_n \end{bmatrix},$$

system (16) becomes

$$\begin{bmatrix} M_{n+1} \\ N_{n+1} \end{bmatrix} = \begin{bmatrix} -1 & 0 \\ 0 & \lambda_2 \end{bmatrix} \begin{bmatrix} M_n \\ N_n \end{bmatrix} + \begin{bmatrix} g_1(u_n, v_n, \bar{\delta}) \\ g_2(u_n, v_n, \bar{\delta}) \end{bmatrix}$$

where

$$g_1(u_n, v_n, \bar{\delta}) = \frac{\lambda_2 - a_{11}}{a_{12}(\lambda_2+1)} f_1(u_n, v_n, \bar{\delta}) - \frac{1}{\lambda_2+1} f_2(u_n, v_n, \bar{\delta})$$
$$g_2(u_n, v_n, \bar{\delta}) = \frac{1+a_{11}}{a_{12}(\lambda_2+1)} f_1(u_n, v_n, \bar{\delta}) + \frac{1}{\lambda_2+1} f_2(u_n, v_n, \bar{\delta})$$

with

$$u_n = a_{12}(M_n + N_n), \qquad v_n = -(1+a_{11})M_n + (\lambda_2 - a_{11})N_n,$$

If the center manifold is supposed to have the form

$$\varphi(M_n, \bar{\delta}) = \nu_1 M_n^2 + \nu_2 M_n\bar{\delta} + \mathcal{O}((|M_n| + |\bar{\delta}|)^3), \tag{17}$$

then function $\varphi(M_n, \bar{\delta})$ needs to fulfill

$$\begin{aligned} \varphi(-M_n + g_1(M_n, \varphi(M_n, \bar{\delta}), \bar{\delta}), \bar{\delta}) - \lambda_2\varphi(M_n, \bar{\delta}) \\ - g_2(M_n, \varphi(M_n, \bar{\delta}), \bar{\delta}) = 0. \end{aligned} \tag{18}$$

When we solve equation (18), we get

$$\begin{aligned} \nu_1 &= \frac{a_{12}^2((a_{11}+1)a_{13} + a_{12}a_{23}) - a_{12}(a_{11}+1)((a_{11}+1)a_{14} + a_{12}a_{24})}{a_{12}(1-\lambda_2^2)} \\ \nu_2 &= \frac{-a_{12}((a_{11}+1)b_1 + a_{12}c_1) + (a_{11}+1)^2 b_2}{a_{12}(\lambda_2+1)^2}. \end{aligned} \tag{19}$$

The system (17) restricted in the center manifold can then be written as

$$\begin{aligned} G(M_n, \bar{\delta}) = &- M_n + \varphi_1 M_n^2 + \varphi_2 M_n\bar{\delta} + \varphi_3 M_n^2\bar{\delta} + \varphi_4 M_n\bar{\delta}^2 \\ &+ \varphi_5 M_n^3 + \mathcal{O}((|M_n| + |\bar{\delta}|)^4) \end{aligned} \tag{20}$$

where

$$\begin{aligned} \varphi_1 = &\frac{a_{12}(a_{11}+1)((\lambda_2 - a_{11})a_{14} - a_{12}a_{24})}{a_{12}(\lambda_2+1)} \\ &- \frac{a_{12}(a_{11}+1)((\lambda_2 - a_{11})a_{14} - a_{12}a_{24})}{a_{12}(\lambda_2+1)} \\ \varphi_2 = &\frac{a_{12}((\lambda_2 - a_{11})b_1 - a_{12}c_1) - b_2(\lambda_2 - a_{11})(a_{11}+1)}{a_{12}(\lambda_2+1)} \\ \varphi_3 = &\frac{2\nu_2 a_{12}^2(\lambda_2 - a_{11}a_{13} - a_{12}a_{23})}{a_{12}(\lambda_2+1)} \\ &+ \frac{\nu_2 a_{12}(\lambda_2 - 2a_{11} - 1)((\lambda_2 - a_{11})a_{14} - a_{12}a_{24})}{a_{12}(\lambda_2+1)} \\ &+ \frac{\nu_1\left(a_{12}((\lambda_2 - a_{11})b_1 - a_{12}c_1) + (\lambda_2 - a_{11})^2 b_2\right)}{a_{12}(\lambda_2+1)} \\ &+ \frac{a_{12}^2((\lambda_2 - a_{11})b_3 - a_{12}c_3)}{a_{12}(\lambda_2+1)} \\ &- \frac{a_{12}(a_{11}+1)((\lambda_2 - a_{11})b_4 - a_{12}c_4)}{a_{12}(\lambda_2+1)} \\ \varphi_4 = &\frac{\nu_2 a_{12}((\lambda_2 - a_{11})b_1 - a_{12}c_1)}{a_{12}(\lambda_2+1)} \\ &+ \frac{\nu_2(\lambda_2 - a_{11})((\lambda_2 - a_{11})b_2 - a_{12}c_2)}{a_{12}(\lambda_2+1)} \\ \varphi_5 = &\frac{2\nu_1 a_{12}^2((\lambda_2 - a_{11})a_{13} - a_{12}a_{23})}{a_{12}(\lambda_2+1)} \\ &+ \frac{\nu_1 a_{12}(\lambda_2 - 2a_{11} - 1)((\lambda_2 - a_{11})a_{14} - a_{12}a_{24})}{a_{12}(\lambda_2+1)} \\ &+ \frac{a_{12}^2((\lambda_2 - a_{11})a_{15} - a_{12}a_{25})}{(\lambda_2+1)}. \end{aligned}$$

To achieve flip bifurcation, both discriminatory quantities (χ_1 and χ_2) must be nonzero, where

$$\begin{aligned} \chi_1 &= \left(\frac{\partial^2 G}{\partial M_n \partial\bar{\delta}} + \frac{1}{2}\frac{\partial G}{\partial\bar{\delta}}\frac{\partial^2 g}{\partial M_n^2}\right)\Big|_{(0,0)} = \varphi_2, \\ \chi_2 &= \left(\frac{1}{6}\frac{\partial^3 G}{\partial M_n^3} + \left(\frac{1}{2}\frac{\partial^2 G}{\partial M_n^2}\right)^2\right)\Big|_{(0,0)} = \varphi_1^2 + \varphi_5. \end{aligned} \tag{21}$$

When the parameter δ varies slightly around $\hat{\delta_1}$, the system (7) undergoes a flip bifurcation at the fixed point $E^* = (x^*, y^*)$ provided that $\chi_2 \neq 0$. Additionally, the period-two orbits that emerge from the fixed point are stable if $\chi_2 > 0$ and unstable if $\chi_2 < 0$.

Neimark-Sacker Bifurcation

From the stability analysis of the fixed point E^*, it is known that for all parameters in Ω_3, where

$$\Omega_3 = \left\{(\alpha, a, b, c, p, q, \delta) \mid \Delta < 0, \delta = \hat{\delta_0}\right\},$$

the Jacobian matrix (13) has two eigenvalues $\lambda_{1,2} \in \mathbb{C}$ with $|\lambda_{1,2}| = 1$. This fact indicates that the discrete system (7) may experience a

NS bifurcation if the parameters experience small perturbations around Ω_3. In this article, the bifurcation will be investigated by introducing a small perturbation $\tilde{\delta} \ll 1$ on the parameter δ around $\delta = \hat{\delta_0}$ so that the system (7) can be written as

$$\begin{aligned} x_{n+1} &= x_n + (\hat{\delta_0} + \tilde{\delta}) \left[(1 - x_n)x_n - \frac{x_n y_n}{a + x_n} - p x_n \right] \\ y_{n+1} &= y_n + (\hat{\delta_0} + \tilde{\delta}) \left[\frac{b x_n y_n}{a + x_n} - (c + q) y_n \right]. \end{aligned} \tag{22}$$

By noticing that $\delta = \hat{\delta_0} \Leftrightarrow h = \hat{h_0}$, the perturbation of δ around $\delta = \hat{\delta_0}$ can also be interpreted as a perturbation of h around $h = \hat{h_0}$. We now take a translation $u_n = x_n - x^*$ and $v_n = y_n - y^*$ such that the discrete system (22) can be written as

$$\begin{aligned} u_{n+1} =& u_n + (\hat{\delta_0} + \tilde{\delta}) \left[(1 - (u_n + x^*))(u_n + x^*) \right] \\ & - (\hat{\delta_0} + \tilde{\delta}) \left[\frac{(u_n + x^*)(v_n + y^*)}{a + (u_n + x^*)} + p(u_n + x^*) \right] \\ v_{n+1} =& v_n + (\hat{\delta_0} + \tilde{\delta}) \left[\frac{b(u_n + x^*)(v_n + y^*)}{a + (u_n + x^*)} - (c + q)(v_n + y^*) \right], \end{aligned} \tag{23}$$

and the fixed point E^* is shifted to the origin $(0, 0)$. It can be shown that the Jacobian matrix of system (23) around the origin has a characteristics equation

$$\lambda^2 + \rho(\tilde{\delta})\lambda + \phi(\tilde{\delta}) = 0, \tag{24}$$

where

$$\begin{aligned} \rho(\tilde{\delta}) &= -2 - (\hat{\delta_0} + \tilde{\delta})\Psi_1, \\ \phi(\tilde{\delta}) &= 1 + (\hat{\delta_0} + \tilde{\delta})\Psi_1 + (\hat{\delta_0} + \tilde{\delta})^2 \Psi_2. \end{aligned}$$

The characteristics roots of equation (24) are

$$\begin{aligned} \lambda_{1,2} =& \frac{1}{2}(-\rho(\tilde{\delta}) \pm \sqrt{\rho(\tilde{\delta})^2 - 4\phi(\tilde{\delta})}) \\ =& \frac{1}{2}(-\rho(\tilde{\delta}) \pm i\sqrt{4\phi(\tilde{\delta}) - \rho(\tilde{\delta})^2}). \end{aligned}$$

It can be shown that those characteristics roots satisfy

$$|\lambda_{1,2}| = \sqrt{\phi(\tilde{\delta})}, \text{ and } \frac{d|\lambda_1|}{d\tilde{\delta}}\Big|_{\tilde{\delta}=0} = \frac{d|\lambda_2|}{d\tilde{\delta}}\Big|_{\tilde{\delta}=0} = -\frac{\Psi_1}{2} > 0.$$

Clearly that if $\tilde{\delta} = 0$ then $\lambda_{1,2}^m \neq 1$, $m = 1, 2, 3, 4$ is equivalent to condition $\rho(0) \neq -2$, 0, 1, 2. From the previous analysis, it was identified that, for all $(a, b, c, p, q, \delta) \in \Omega$, $\phi(0) = 1 + \hat{\delta_0}\Psi_1 + \hat{\delta_0}^2\Psi_2 = 1$, and therefore $\rho(0)^2 - 4\phi(0) < 0$ or $\rho(0)^2 < 4\phi(0) = 4$. Consequently that $\rho(0) \neq \pm 2$. Furthermore, we can also prove that

$$\rho(0) = -2 - \hat{\delta_0}\Psi_1 = -2 - \left(-\frac{\Psi_1}{\Psi_2}\Psi_1 \right) = -2 + \frac{\Psi_1^2}{\Psi_2}.$$

Thus, $\rho(0) \neq 0, 1$ is achieved whenever $\Psi_1^2/\Psi_2 \neq 2, 3$.

By denoting $\mu = \mathrm{Re}(\lambda_{1,2}|_{\tilde{\delta}=0})$ and $\gamma = \mathrm{Im}(\lambda_{1,2}|_{\tilde{\delta}=0})$, i.e.,

$$\mu = -\frac{\rho(0)}{2} = 1 - \frac{\hat{\delta_0}\Psi_1}{2}, \quad \gamma = \frac{\sqrt{4\phi(0) - \rho(0)^2}}{2} = \frac{\hat{\delta_0}}{2}\sqrt{-\Delta},$$

We now form a normal form of system (23). Using a transformation

$$\begin{bmatrix} u_n \\ v_n \end{bmatrix} = \begin{bmatrix} a_{12} & 0 \\ \mu - a_{11} & -\gamma \end{bmatrix} \begin{bmatrix} M_n \\ N_n \end{bmatrix},$$

system (23) is transformed to

$$\begin{bmatrix} M_{n+1} \\ N_{n+1} \end{bmatrix} = \begin{bmatrix} \mu & -\gamma \\ \gamma & \mu \end{bmatrix} \begin{bmatrix} M_n \\ N_n \end{bmatrix} + \begin{bmatrix} \tilde{g_1}(M_n, N_n) \\ \tilde{g_2}(M_n, N_n) \end{bmatrix}, \tag{25}$$

where

$$\begin{aligned} \tilde{g_1}(M_n, N_n) =& \frac{1}{a_{12}} \left(a_{13}u_n^2 + a_{14}u_n v_n + a_{15}u_n^3 + a_{16}u_n^2 v_n \right) \\ & + \mathcal{O}((|M_n| + |N_n|)^4), \\ \tilde{g_2}(M_n, N_n) =& \frac{1}{a_{12}\gamma} \left((\mu - a_{11})a_{13} - a_{12}a_{23} \right) u_n^2 \\ & + \frac{1}{a_{12}\gamma} \left((\mu - a_{11})a_{14} - a_{12}a_{24} \right) u_n v_n \\ & + \frac{1}{a_{12}\gamma} \left((\mu - a_{11})a_{15} - a_{12}a_{25} \right) u_n^3 \\ & + \frac{1}{a_{12}\gamma} \left((\mu - a_{11})a_{16} - a_{12}a_{26} \right) u_n^2 v_n \\ & + \mathcal{O}((|M_n| + |N_n|)^4), \end{aligned} \tag{26}$$

with

$$u_n = a_{12}M_n, \quad v_n = (\mu - a_{11})M_n + \gamma N_n.$$

$a_{ij}, \forall i, j$ in equations (26) are the same as in (16), except that $\hat{\delta_1} = \hat{\delta_0} + \tilde{\delta}$. From equations (26), we have that

$$\begin{aligned} \frac{\partial^2 \tilde{g_1}}{\partial M_n^2} =& 2(a_{12}a_{13} + (\mu - a_{11})a_{14}), \\ \frac{\partial^2 \tilde{g_1}}{\partial M_n \partial N_n} =& -\gamma a_{14}, \quad \frac{\partial^2 \tilde{g_1}}{\partial N_n^2} = 0, \\ \frac{\partial^3 \tilde{g_1}}{\partial M_n^3} =& (a_{12}^2 a_{15} + a_{12}a_{16}(\mu - a_{11})), \\ \frac{\partial^3 \tilde{g_1}}{\partial M_n^2 \partial N_n} =& -2a_{12}a_{16}\gamma, \\ \frac{\partial^3 \tilde{g_1}}{\partial M_n \partial N_n^2} =& \frac{\partial^3 \tilde{g_1}}{\partial N_n^3} = 0, \\ \frac{\partial^2 \tilde{g_2}}{\partial M_n^2} =& \frac{2}{\gamma} \left[a_{12}((\mu - a_{11})a_{13} - a_{12}a_{23}) \right] \\ & + \frac{2}{\gamma} \left[(\mu - a_{11})((\mu - a_{11})a_{14} - a_{12}a_{24}) \right], \\ \frac{\partial^2 \tilde{g_2}}{\partial M_n \partial N_n} =& -(\mu - a_{11})a_{14} + a_{12}a_{24}, \\ \frac{\partial^3 \tilde{g_2}}{\partial N_n^2} =& 0, \\ \frac{\partial^3 \tilde{g_2}}{\partial M_n^3} =& \frac{6}{\gamma} \left[a_{12}^2((\mu - a_{11})a_{15} - a_{12}a_{25}) \right] \\ & + \frac{6}{\gamma} \left[a_{12}((\mu - a_{11})a_{16} - a_{12}a_{26}) \right] \\ \frac{\partial^3 \tilde{g_2}}{\partial M_n^2 \partial N_n} =& -2a_{12} \left[((\mu - a_{11})a_{16} - a_{12}a_{26}) \right], \\ \frac{\partial^3 \tilde{g_2}}{\partial M_n \partial N_n^2} =& \frac{\partial^3 \tilde{g_2}}{\partial N_n^3} = 0. \end{aligned}$$

The discrete system 7 will experiences a NS bifurcation if the quantity χ^* is nonzero, i.e.,

$$\chi^* = -\mathrm{Re}\left(\frac{(1 - 2\bar{\lambda})\bar{\lambda}^2}{1 - \lambda} \xi_{11}\xi_{20} \right) - \frac{1}{2}|\xi_{11}|^2 - |\xi_{02}|^2 + \mathrm{Re}(\bar{\lambda}\xi_{21}) \neq 0,$$

where

$$\xi_{02} = \frac{1}{8}\left[\frac{\partial^2 \tilde{g}_1}{\partial M_n^2} - \frac{\partial^2 \tilde{g}_1}{\partial N_n^2} + 2\frac{\partial^2 \tilde{g}_2}{\partial M_n \partial N_n} + i\left(\frac{\partial^2 \tilde{g}_2}{\partial M_n^2} - \frac{\partial^2 \tilde{g}_2}{\partial N_n^2} + 2\frac{\partial^2 \tilde{g}_1}{\partial M_n \partial N_n}\right)\right],$$

$$\xi_{11} = \frac{1}{4}\left[\frac{\partial^2 \tilde{g}_1}{\partial M_n^2} + \frac{\partial^2 \tilde{g}_1}{\partial N_n^2} + i\left(\frac{\partial^2 \tilde{g}_2}{\partial M_n^2} + \frac{\partial^2 \tilde{g}_2}{\partial N_n^2}\right)\right],$$

$$\xi_{20} = \frac{1}{8}\left[\frac{\partial^2 \tilde{g}_1}{\partial M_n^2} - \frac{\partial^2 \tilde{g}_1}{\partial N_n^2} + 2\frac{\partial^2 \tilde{g}_2}{\partial M_n \partial N_n} + i\left(\frac{\partial^2 \tilde{g}_2}{\partial M_n^2} - \frac{\partial^2 \tilde{g}_2}{\partial N_n^2} - 2\frac{\partial^2 \tilde{g}_1}{\partial M_n \partial N_n}\right)\right],$$

$$\xi_{21} = \frac{1}{16}\left[\frac{\partial^3 \tilde{g}_1}{\partial M_n^3} + \frac{\partial^3 \tilde{g}_1}{\partial M_n \partial N_n^2} + \frac{\partial^3 \tilde{g}_2}{\partial M_n^2 \partial N_n} + \frac{\partial^3 \tilde{g}_2}{\partial N_n^3}\right] + i\frac{1}{16}\left[\frac{\partial^3 \tilde{g}_2}{\partial M_n^3} + \frac{\partial^3 \tilde{g}_2}{\partial M_n \partial N_n^2} - \frac{\partial^3 \tilde{g}_1}{\partial M_n^2 \partial N_n} - \frac{\partial^3 \tilde{g}_1}{\partial N_n^3}\right].$$

Moreover, the NS bifurcation is supercritical (subcritical) if $\chi^* < 0$ ($\chi^* > 0$).

CHAOS CONTROL

A system with optimal performance and no chaos is always desired in dynamic systems. The process of applying small perturbations to a specific system in order to stabilize periodic orbits is known as controlling chaos. The goal of chaos control strategies is to stabilize and predict chaotic activity. There are numerous methods for managing chaos in the discrete time model. Two forms of chaos control — hybrid control and state feedback control — will be implemented in this study.

Hybrid control strategy

By assuming that the model (7) experiences a flip or NS bifurcation at a fixed point E^*, we follow (Panigoro *et al.* 2023; Ruan and Li 2024) to implement a hybrid control to the system (7) such that we get

$$\begin{aligned} x_{n+1} &= \sigma\left(x_n + \delta\left((1-x_n)x_n - \frac{x_n y_n}{a+x_n} - p x_n\right)\right) + (1-\sigma)x_n \\ y_{n+1} &= \sigma\left(y_n + \delta\left(\frac{b x_n y_n}{a+x_n} - (c+q)y_n\right)\right) + (1-\sigma)y_n \end{aligned} \tag{27}$$

with control parameter $\sigma \in (0,1)$. It is easily verified that model (27) has exactly the same fixed points as uncontrol model (7). The Jacobian matrix of system (27) at the fixed point E^* is

$$J_c(E^*) = \begin{bmatrix} 1+\delta\sigma j_{11} & \delta\sigma j_{12} \\ \delta\sigma j_{21} & 1 \end{bmatrix}, \tag{28}$$

where

$$\begin{aligned} j_{11} &= \frac{(c+q)}{b(b-(c+q))}((1-p)(b-(c+q)) - a(b+c+q)), \\ j_{12} &= -\frac{c+q}{b} < 0, \\ j_{21} &= (1-p)(b-(c+q)) - a(c+q). \end{aligned}$$

The eigenvalues of Jacobian matrix (28) can be analyzed using the same method as that of Jacobian matrix (13) since those two matrices are very similar. In this way, we can show that if $1-p < L^* + \frac{ab}{b-(c+q)}$ then the fixed point E^* is asymptotically stable if one of the following conditions holds:

1. $\Delta < 0$ and $0 < h < \tilde{h_0}$, where $\tilde{h_0} = \frac{\hat{h_0}}{\sqrt[\alpha]{\sigma}} = \sqrt[\alpha]{\frac{\alpha\Gamma(\alpha)\delta_0}{\sigma}}$; or
2. $\Delta \geq 0$ and $0 < h < \tilde{h_1}$, where $\tilde{h_1} = \frac{\hat{h_1}}{\sqrt[\alpha]{\sigma}} = \sqrt[\alpha]{\frac{\alpha\Gamma(\alpha)\delta_1}{\sigma}}$.

It can be seen that the fixed point E^* of the system with hybrid control (27) has a wider stability region compared to the uncontrol system (7). Without hybrid control, the fixed point E^* of model (7) loses its stability when h passes $\hat{h_0}$ (for the case of $\Delta < 0$) or $\hat{h_1}$ (for the case of $\Delta > 0$). On the other hand, the appearance of a hybrid control in the system with control parameter σ leads to a shifting of the critical value of h. Indeed, the fixed point E^* of the control system (27) is asymtotically stable if $h < \frac{\hat{h_0}}{\sqrt[\alpha]{\sigma}}$ (for the case of $\Delta < 0$) or $h < \frac{\hat{h_1}}{\sqrt[\alpha]{\sigma}}$ (for the case of $\Delta > 0$), dengan $0 < \sigma < 1$. Henceforth, if the fixed point E^* of model (7) with a specific time step h is unstable and the system experiences chaotic behaviour then the chaos can be controlled by implementing a hybrid control to the system with control parameter $\sigma \in \left(0, -\frac{\alpha\Gamma(\alpha)A}{h^\alpha B}\right)$ (or $\sigma \in \left(0, -\frac{\alpha\Gamma(\alpha)(A+\sqrt{\Delta})}{h^\alpha B}\right)$) if $\Delta < 0$ (or $\Delta \geq 0$).

State Feedback Control

By following (Ruan and Li 2024; Khan *et al.* 2024; Li *et al.* 2024), a state feedback control will be employed in this part to stabilize chaotic orbits at a fixed point E^* of unstable systems (7). With this state feedback control, model (7) becomes

$$\begin{aligned} x_{n+1} &= x_n + \delta\left((1-x_n)x_n - \frac{x_n y_n}{a+x_n} - p x_n\right) + z_n \\ y_{n+1} &= y_n + \delta\left(\frac{b x_n y_n}{a+x_n} - (c+q)y_n\right), \end{aligned} \tag{29}$$

where $z_n = -\omega_1(x_n - x^*) - \omega_2(y_n - y^*)$ denotes the strength of the feedback control, while ω_1 and ω_2 denote the feedback gain. It is evident that the fixed points of the uncontrolled model (7) and the (29) model are identical. At the fixed point E^*, the Jacobian matrix of system (29) is

$$J_{fb}(E^*) = \begin{bmatrix} 1+\delta j_{11} - \omega_1 & \delta j_{12} - \omega_2 \\ \delta j_{21} & 1 \end{bmatrix}, \tag{30}$$

where j_{11}, j_{12} and j_{21} are exactly the same as in matrix (13).

The eigenvalues of the Jacobian matrix (30) can be determined by solving the following characteristics equation

$$\lambda^2 - Tr(J_{fb}(E^*))\lambda + Det(J_{fb}(E^*)) = 0 \tag{31}$$

where

$$\begin{aligned} Tr(J_{fb}(E^*)) &= 2 + \Psi_1\delta - \omega_1, \\ Det(J_{fb}(E^*)) &= 1 + \Psi_1\delta + \Psi_2\delta^2 - \omega_1 + \omega_2\delta j_{21}, \end{aligned}$$

and

$$\Psi_1 = j_{11} \quad \text{and} \quad \Psi_2 = -j_{12}j_{21}.$$

Let λ_1 and λ_2 are the eigenvalues of matrix (30). Then,

$$\begin{aligned} \lambda_1 + \lambda_2 &= 2 + \Psi_1\delta - \omega_1, \\ \lambda_1\lambda_2 &= 1 + \Psi_1\delta + \Psi_2\delta^2 - \omega_1 + \omega_2\delta j_{21}. \end{aligned} \tag{32}$$

It is necessary to solve equations $\lambda_1 = \pm 1$ and $\lambda_1\lambda_2 = 1$ in order to determine the marginal stability lines of the fixed E^*. The purpose of this constraint is to guarantee that $|\lambda_{1,2}| < 1$. Assuming $\lambda_1\lambda_2 =$

1, the second part of equation (32) gives the first stability boundary line as follows

$$\mathcal{L}_1 \equiv \omega_1 - \omega_2\delta j_{21} = \Psi_1\delta + \Psi_2\delta^2. \tag{33}$$

Next, the second stability boundary line can be generated by taking $\lambda_1 = 1$, which together with equation (32), yields

$$\mathcal{L}_2 \equiv \omega_2 = \delta j_{12}. \tag{34}$$

Finally we suppose that $\lambda_1 = -1$. Then, by equation (32) we get

$$\mathcal{L}_3 \equiv 2\omega_1 - \omega_2\delta j_{21} = 4 + 2\Psi_1\delta + \Psi_2\delta^2. \tag{35}$$

We remark that if ω_1 and ω_2 lie in the triangular region bounded by lines $\mathcal{L}_1, \mathcal{L}_2$ and $\mathcal{L}_3$, then the fixed point E^* of the system (29) is asymptotically stable.

NUMERICAL SIMULATIONS

In this section, we present several numerical simulations to demonstrate and validate the earlier analytical findings. It should be mentioned that since the real-life parameter values are unavailable, we utilize the hypothetical ones. As an illustration, we initially select the following parameters.

$$\alpha = 0.7, a = 2, b = 1, c = 0.2, p = 0.1, q = 0.1, \tag{36}$$

and vary the parameter $h \in [2.5, 4.8]$. The initial condition for this simulation is $x(0) = 0.2, y(0) = 0.1$. In this particular case, $E^*(0.8571,\ 0.1224)$ is the interior fixed point of the system (7). Our calculations outcomes show that $\Delta = 0.6768 > 0, \hat{\delta_1} = 2.3996$, and $\hat{h_1} = 3.0451$. Thus, in the present situation, the parameter $(\alpha, a, b, d, p, q) \in \Omega_1$ leads to a flip (period-doubling) bifurcation. More specifically, if $h < \hat{h_1}$ then the fixed point $E^*(0.8571,\ 0.1224)$ is asymptotically stable; while if h exceeds $\hat{h_1}$ then stability is lost.

The discriminatory quantities $\chi_1 = -0.8335$ and $\chi_2 = -0.6074$ are non-zero which indicate the occurrence of flip bifurcation. The flip bifurcation is unstable since $\chi_2 < 0$. The bifurcation diagram in the (h, x^*)–plane, shown in Figure 1.(a-b), provides a vivid illustration of this bifurcation phenomena. Figure 1.(a) depicts that after the bifurcation parameter (h) crosses the value of $\hat{h_1}$, there occurs a period-doubling cascade in orbits of period-2, 4, 8, and 16 as well quasi-periodic and even chaotic orbits for the solution x_n. However, such phenomenon is not observed in (h, y^*)-plane due to y_n always converges to 0 for $h > \hat{h_1}$, see Figure 1.(b). The presence of converging orbit (E^* is asymptotically stable), period-doubling orbits, chaotic regions is confirmed by the maximal Lyapunov exponents corresponding to Figure 1.(a-b) shown in Figure 1.(c). It is seen that the maximum value of Lyapunov exponent are positive for some intervals of h, which characterizes the occurrence of chaos. Figure 2 illustrates this point by displaying many temporal solutions of x_n for a range of h values. For $h < \hat{h_1}$, it is seen that the x_n converges to x^*; however, for $h > \hat{h_1}$, x may converge to the orbits of period-2,-3,-4, -5, etc., or it may behave chaotically.

It is evident from Figures 1 and 2 that chaos may occur in the model (7) with parameters (36). The model (7) can be subjected to a hybrid control in attempt to control chaotic events. For instance, Figure 3.(a-b) demonstrates that the fixed point $E^*(0.8571,\ 0.1224)$ of model (7) with $h = 3.96$ is unstable. In this case, a chaotic orbit for x_n is generated, while x_n is convergent to 0. On the other hand, if a hybrid control is applied as in the model (27), then the eigenvalues of the Jacobian matrix (28) are in the stability region ($|\lambda_{1,2}| < 1$) if $\sigma \in (0,\ 0.832)$. The graphs of x_n and y_n of the controlled model (27) with $\sigma = 0.8$ and initial value $x(0) = 0.2, y(0) = 0.8$ are displayed in Figure 3.(c-d). It is clearly evident that the fixed point E^* is now asymptotically stable.

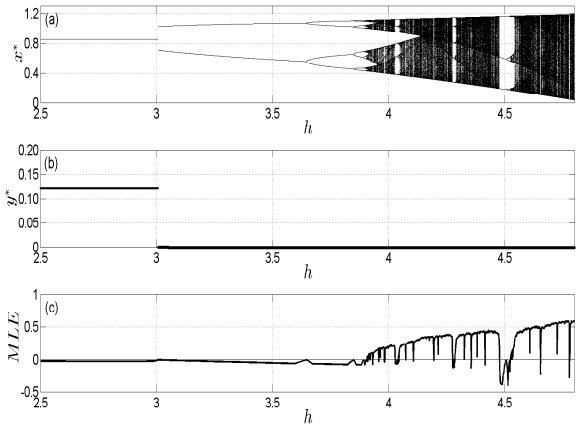

Figure 1 Bifurcation diagrams in (a) (h, x^*)–plane, (b) (h, y^*)–plane, and (c) the corresponding maximum Lyapunov exponent (MLE) of system (7) with $\alpha = 0.7, a = 2, b = 1, c = 0.2, p = 0.1, q = 0.1$, and $h \in [2.5, 4.8]$.

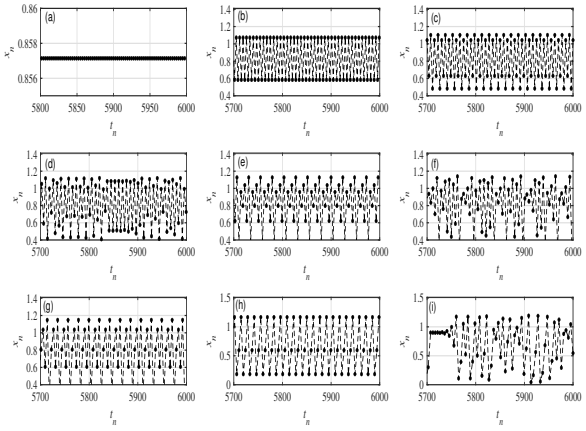

Figure 2 Temporal solution of x_n for system (7) with $\alpha = 0.7, a = 2, b = 1, c = 0.2, p = 0.1$, and $q = 0.1$ around $t = 6000$, for different valus of h: (a) $h = 2.8$, (b) $h = 3.5$, (c) $h = 3.75$, (d) $h = 3.96$, (e) $h = 4.03$, (f) $h = 4.2$, (g) $h = 4.28$, (h) $h = 4.5$, (i) $h = 4.8$.

If the model (3) with parameters (36) is subjected to a state feedback control as in the system (29), we obtain three boundary lines for the stability region, namely

$$\begin{aligned}
\mathcal{L}_1 &\equiv -\omega_1 + 0.0865\omega_2 = 2.3601,\\
\mathcal{L}_2 &\equiv \omega_2 = -0.8659,\\
\mathcal{L}_3 &\equiv -2\omega_1 + 0.0865\omega_2 = 0.7950.
\end{aligned}$$

Figure 4 displays the stable triangular area in the (ω_1, ω_2)–plane for the controlled system (29) that is bounded by the marginal lines $\mathcal{L}_1, \mathcal{L}_2$ and $\mathcal{L}_3$. We have included a numerical simulation to show how the feedback method operates and controls chaos in unstable states. As in previous example, we take parameters (36) and $h = 3.96$. The feedback gains are $\omega_1 = -0.75$ and $\omega_2 = -0.7$, with the initial value being $(x(0), y(0)) = (0.2, 0.8)$. The chaotic

trajectory is now stabilized at the fixed point $E^*(0.8571,\ 0.1224)$, as shown in Figure 3.(e-f).

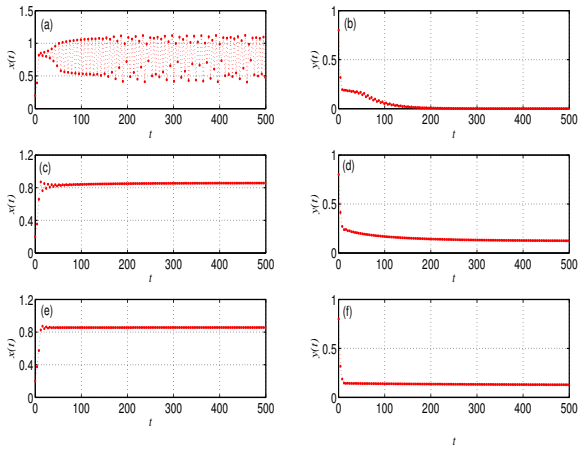

Figure 3 Temporal solution for system (7) with $\alpha = 0.7, a = 2, b = 1, c = 0.2, p = 0.1, q = 0.1, h = 3.96$; and initial value $(x(0), y(0)) = (0.2, 0.8)$. The first column depicts the solution of x_n, while the second column shows the solution of y_n: (a-b) without control, (c-d) with hybrid control where $\sigma = 0.8$, and (e-f) with state feedback control where $\omega_1 = -0.75$ and $\omega_2 = -0.7$.

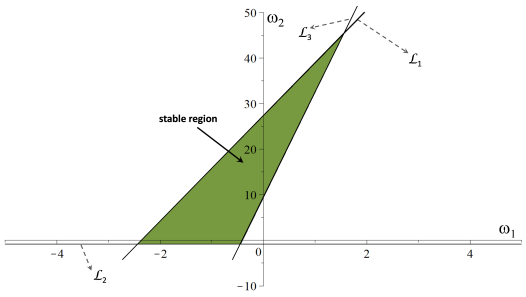

Figure 4 Stability region for system with state feedback control (29) with $\alpha = 0.7, a = 2, b = 1, c = 0.2, p = 0.1, q = 0.1$, and $h = 3.96$.

For the subsequent simulation, the following parameter values are used:

$$\alpha = 0.9, a = 1, b = 1, c = 0.2, p = 0.3, q = 0.05, \tag{37}$$

and $h \in [3.4, 5.2]$. It is evident that the simulation's parameters fall into Ω_3, where $\delta_0 = 3.5151$ and $\Delta = -0.2166 < 0$. We also observe that $h = \hat{h_0}$ is equivalent to $\delta = \delta_0$. Here, the fixed point $E^*(0.3333, 0.4889)$ of the system (7) is stable if $h < \hat{h_0} = 3.8707$. When the system (7) is linearized around a fixed point E^*, the eigenvalues of the resulting Jacobian matrix are $\lambda_{1,2} = \mu \pm \gamma i$ and $|\lambda_{1,2}| = 1$, with $\mu = 0.57525$ and $\gamma = 0.81798$. In addition, it is found that $\rho(0) = -1.1505 \neq \pm 1$ and $\chi^* = -1.3642 < 0$. Therefore, the system (7) experiences a stable Neimark-Sacker bifurcation around E^* when h passes $h = \hat{h_0}$. This is indicated by the appearance of closed invariant curves when $h > \hat{h_0}$. This phenomenon is clearly seen in the bifurcation diagrams in (h, x^*)–plane and (h, y^*), see Figure 5.(a-b), as well as in the phase-portrait in Figure 6. The system also experiences the chaos phenomena, as evidenced by the positive value of the maximal Lyapunov exponent shown in Figure 5.(c).

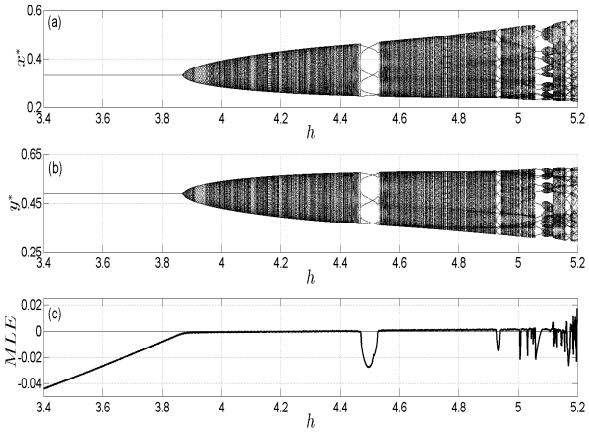

Figure 5 Bifurcation diagrams in (a) (h, x^*)–plane, (b) (h, y^*)–plane, and (c) the corresponding maximum Lyapunov exponent (MLE) of system (7) with $\alpha = 0.9, a = 1, b = 1, c = 0.2, p = 0.3, q = 0.05$, and $h \in [3.4, 5.2]$.

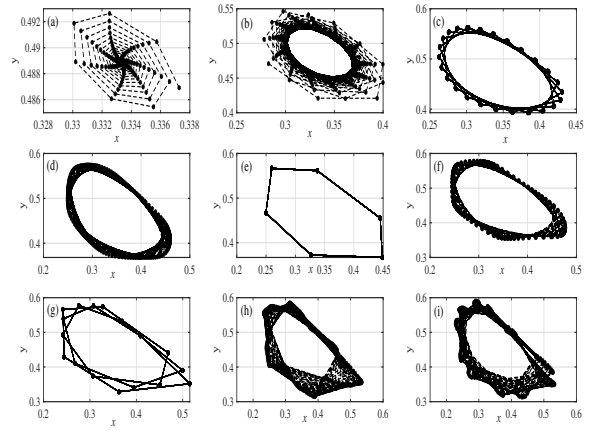

Figure 6 Phase portrait for system (7) with $\alpha = 0.9, a = 1, b = 1, c = 0.2, p = 0.3, q = 0.05$, and (a) $h = 3.6$, (b) $h = 3.93$, (c) $h = 4.2$, (d) $h = 4.44$, (e) $h = 4.5$, (f) $h = 4.6$, (g) $h = 4.93$, (h) $h = 5$, (i) $h = 5.1$.

It can be seen in Figures 5 and 6 that the model (7) with parameters (37) may lead to chaotic behavior. Similar to the previous example, feedback control or hybrid control can be used to manage this chaotic phenomenon. For instance, when $h = 5.1$, the model (7) produces a chaotic orbit, see Figure 7).(a–b). If a hybrid control is now implemented to the system (7), the fixed point E^* will certainly be asymptotically stable if $\sigma \in (0,\ 0.78)$. To illustrate this, Figures 7.(c-d) depict the trajectories of x_n and y_n which converge to the fixed point E^* when $\sigma = 0.75$ is utilized. Alternatively, by applying a state feedback control to the model (7) with parameters (37) and $h = 5.1$ results in a triangle-stability region for the fixed point E^*, see Figure 8. The marginal lines for the stability region are as follows

$$\begin{aligned}
\mathcal{L}_1 &\equiv -\omega_1 + 1.2390\omega_2 = -0.3068,\\
\mathcal{L}_2 &\equiv \omega_2 = -1.1264,\\
\mathcal{L}_3 &\equiv -2\omega_1 + 1.2390\omega_2 = -3.2179.
\end{aligned}$$

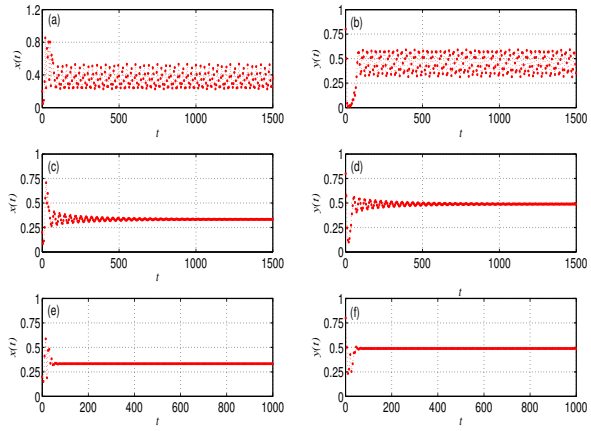

Figure 7 Temporal solution for system (7) with $\alpha = 0.9, a = 1, b = 1, c = 0.2, p = 0.3, q = 0.05, h = 5.1$; and initial value $(x(0), y(0)) = (0.2, 0.8)$. The first column depicts the solution of x_n, while the second column shows the solution of y_n: (a-b) without control, (c-d) with hybrid control where $\sigma = 0.75$, and (e-f) with state feedback control where $\omega_1 = 1$ and $\omega_2 = 0.1$.

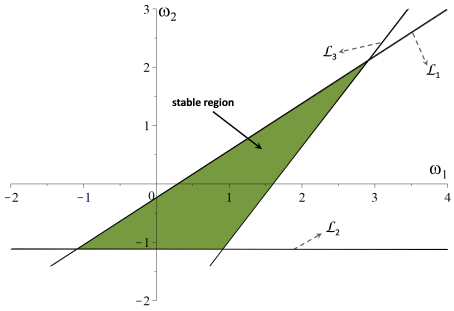

Figure 8 Stability region for system with state feedback control (29) with $\alpha = 0.9, a = 1, b = 1, c = 0.2, p = 0.3, q = 0.05$, and $h = 5.1$.

Hence, if ω_1 and ω_2 are chosen in the stability region, then the fixed point E^* is guaranteed to be asymptotically stable. As an illustration, we plot in Figure 7.(e-f) the temporal solution of x_n and y_n under the state feedback control with $\omega_1 = 1$ and $\omega_2 = 0.1$. It is observed that the solution converges to E^*, confirming the fixed point E^* is asymptotically stable.

To see the influence of harvesting rate of prey population on the dynamics of the model (7), a simulation was carried out by taking fixed parameters $\alpha = 0.9, a = 1, c = 0.2, q = 0.05, h = 4$, and varying $b \in [0.8, 1.2]$ for different value of p. We can clearly observe in Figure 9 that p has a substantial effect on the dynamics of predator-prey populations. The bifurcation diagrams illustrated in Figure 9.(a-d) indicate that the predator-prey system experiences a Neimark-Sacker bifurcation. It is important to note that $p = \frac{\beta}{rm}$ where β represents the conversion rate of predation, r denotes the intrinsic growth rate of prey, and m signifies the handling time required to capture and consume the prey population.

A greater value of p can be achieved by increasing the value of β or reducing the values of r or m. As long as $0 < p < 1$, an increase in p will cause the bifurcation threshold to move to a higher critical value of b. With r and m held constant, this suggests that raising the rate of prey harvesting will enhance the system's

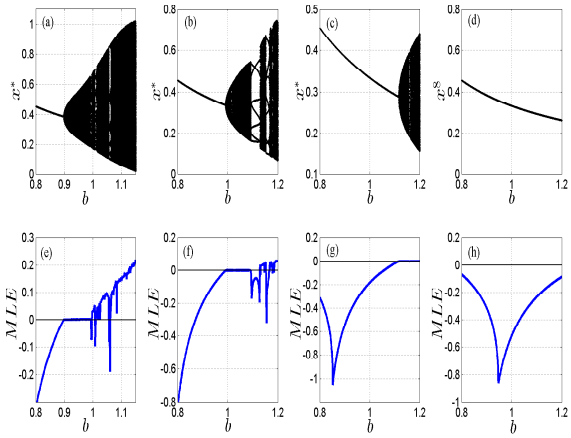

Figure 9 Bifurcation diagram in (b, x^*)–plane when (a) $p = 0.2$, (b) $p = 0.3$, (c) $p = 0.4$, (d) $p = 0.5$; and (e-h) the corresponding maximum Lyapunov exponent (MLE) of system (7) with $\alpha = 0.9, a = 1, c = 0.2, q = 0.05$, and $h = 4$.

stability and help avoid chaotic dynamics. This dynamic behavior can also be observed in the graph of the maximum Lyapunov exponent associated with the bifurcation diagram, see Figure 9.(e-h). However, based on the existence and stability of the fixed points described in the previous section, both prey and predator populations will become extinct if $p \geq 1$.

We have shown analytically and numerically that our proposed discrete model (7) has complex dynamics. In this scenario, the proposed model could reveal flip bifurcation, Neimark-Sacker bifurcation or chaotic behavior. Since the corresponding continuous model, as demonstrated by Sarkar and Mondal (2023), does not exhibit flip bifurcation or chaotic characteristics, this illustrates that the discrete model possesses more complex dynamics compared to its continuous counterpart. Consequently, the discrete model may effectively capture ecological phenomena with a wider range of applicability.

The fact that the discrete model can undergo flip bifurcation suggests that the system can experience period-doubling or even chaotic behavior, as shown in Figures 1 and 2. As mentioned by Eskandari *et al.* (2024), period-doubling bifurcation can cause an increase in the magnitude of population cycles, resulting in more significant fluctuations in population numbers. This can have a major impact on the balance of ecosystems, as increasing changes in population size can increase competition for resources, increase predation rates, and alter various ecological interactions. Apart from that, the occurrence of a flip bifurcation can cause chaos in the dynamics of the population cycle. Such unpredictable behavior can trigger sudden transformations in ecosystems, hindering the development of effective conservation and management strategies. Besides that, the presence of chaos in this context signifies that the predator-prey interaction represented by (7) is unstable. Specifically, as shown by Figure 2, if the prey population falls into a period-doubling state or a chaotic state, the predator species will ultimately face extinction.

The predator-prey discrete model (7) demonstrates the presence of the Neimark-Sacker bifurcation, which signifies the shift from a stable interior point to behaviors that are periodic, quasi-periodic, and even chaotic. Periodic behavior has significant ecological consequences, particularly in terms of recurring population fluc-

tuations between predators and prey about a certain level. Quasi-periodic behavior reflects more intricate, non-repetitive ecological cycles. In both scenarios, predators and prey can coexist while sustaining their individual population densities. The pattern of recurring population cycles simplifies the task of predicting and managing their population dynamics. Conversely, non-repeating population cycles, especially chaotic ones, can complicate predictions of population size changes, thereby hindering the formulation of effective conservation and management strategies.

CONCLUSION

We investigated the complex dynamics of a discrete-time predator-prey model involving harvesting in both prey and predator populations that is constructed from the PWCA approach. The obtained discrete-time model has three fixed points: the extinction of both populations (E_0), the extinction of the predator population (E_1), and the interior point (E^*). Every fixed point is under certain conditions. Our investigation reveals that the discrete-time model experiences flip bifurcation and Neimark-Sacker bifurcation, which are determined by the step size of numerical integration (h). When a flip bifurcation occurs, a period-doubling cascade emerges in orbits with periods of 2, 4, 8, and 16, as well as chaotic orbits around the fixed point E^* after the value of h crosses the critical value. However, for the case of Neimark-Sacker bifurcation, periodic or quasi-periodic orbits as well as chaotic orbits will present when h is larger than the critical value. We showed that the hybrid control or the state feedback control effectively suppresses the chaotic or unstable behaviors. Several computer simulations have confirmed those analytical findings. It is important to mention that the simulations conducted in this article rely on hypothetical parameter values. For future research, it is advisable to examine the proposed discrete model utilizing actual data from chosen ecological cases.

Acknowledgments

This research was funded by Directorate of Research, Technology and Community Service of the Ministry of Education, Culture, Research, and Technology of the Republic of Indonesia through Regular Fundamental Research (PFR) [Contract no. 00309.11/UN10.A0501/B/PT.01.03.2/2024].

Availability of data and material

Not applicable.

Conflicts of interest

The authors declare that there is no conflict of interest regarding the publication of this paper.

LITERATURE CITED

Al-Nassir, S., 2021 Dynamic analysis of a harvested fractional-order biological system with its discretization. Chaos, Solitons & Fractals **152**: 111308.

Alzabut, J., A. G. M. Selvam, V. Dhakshinamoorthy, H. Mohammadi, and S. Rezapour, 2022 On chaos of discrete time fractional order host–immune–tumor cells interaction model. Journal of Applied Mathematics and Computing **68**: 4795–4820.

Arias, C. F., G. Blé, and M. Falconi, 2022 Dynamics of a discrete–time predator–prey system with holling ii functional response. Qualitative Theory of Dynamical Systems **21**: 31.

Beretta, E. and Y. Kuang, 1998 Global analysis in some delayed ratio–dependent predator–prey systems. Nonlinear Analysis: Theory, Methods & Applications **32**: 381–408.

Berryman, A. A., 1992 The origin and evolution of predator–prey theory. Ecology **73**: 1530–1535.

Brown, D. H., H. Ferris, S. Fu, and R. Plant, 2004 Modeling direct positive feedback between predators and prey. Theoretical Population Biology **65**: 143–152.

El-Sayed, A. M. A. and S. M. Salman, 2013 On a discretization process of fractional order riccati differential equation. Journal of Fractional Calculus and Applications **4**: 251–259.

Eskandari, Z., P. A. Naik, and M. Yavuz, 2024 Dynamical behaviors of a discrete–time prey–predator model with harvesting effect on the predator. Journal of Applied Analysis and Computation **14**: 283–297.

Guo, H., J. Han, and G. Zhang, 2023 Hopf bifurcation and control for the bioeconomic predator–prey model with square root functional response and nonlinear prey harvesting. Mathematics **11**: 4958.

Hasan, N., A. Suryanto, and Trisilowati, 2022 Dynamics of a fractional-order eco-epidemic model with Allee effect and refuge on prey. Communications in Mathematical Biology and Neuroscience **2022**: 117.

Holling, C., 1965 The functional response of predators to prey density and its role in mimicry and population regulation. The Memoirs of the Entomological Society of Canada **97**: 5–60.

Holling, C., 1966 The functional response of predators to prey density and its role in mimicry and population regulation. The Memoirs of the Entomological Society of Canada **98**: 5–86.

Khan, A. Q., I. M. Alsulami, and S. K. A. Hamdani, 2024 Controlling the chaos and bifurcations of a discrete prey–predator model. AIMS Mathematics **9**: 1783–1818.

Khan, M. S., M. A. Khan, M. S. Shabbir, and Q. Din, 2019 Stability, bifurcation and chaos control in a discrete–time prey–predator model with holling type-ii response. Network Biology **9**: 55–77.

Lee, J. and H. Baek, 2017 Dynamics of a Beddington–De Angelis–type predator–prey system with constant rate harvesting. Electronic Journal of Qualitative Theory of Differential Equations **2017**: 1–20.

Li, W., C. Zhang, and M. Wang, 2024 Analysis of the dynamical properties of discrete predator–prey systems with fear effects and refuges. Discrete Dynamics in Nature and Society **2024**: 9185585.

Liu, X. and D. Xiao, 2007 Complex dynamic behaviors of a discrete-time predator-prey system. Chaos, Solitons & Fractals **32**: 80–94.

Liu, Y. and X. Li, 2021 Dynamics of a discrete predator-prey model with holling-ii functional response. International Journal of Biomathematics **14**: 2150068.

Mandal, G., L. N. Guin, S. Chakravarty, and R. Han, 2025 Dynamic complexities in a predator–prey model with prey refuge influenced by double Allee effects. Mathematics and Computers in Simulation **227**: 527–552.

Mondal, B., U. Ghosh, S. Sarkar, and P. K. Tiwari, 2024 A generalist predator–prey system with the effects of fear and refuge in deterministic and stochastic environments. Mathematics and Computers in Simulation **225**: 968–991.

Mondal, S., M. Biswas, and N. Bairagi, 2020 Local and global dynamics of a fractional–order predator–prey system with habitat complexity and the corresponding discretized fractional-order system. Journal of Applied Mathematics and Computing **63**: 311–340.

Mukhopadhyay, B. and R. Bhattacharyya, 2016 Effects of harvesting and predator interference in a model of two-predators competing for a single prey. Applied Mathematical Modelling **40**: 3264–3274.

Panigoro, H. S., M. Rayungsari, and A. Suryanto, 2023 Bifurcation and chaos in a discrete–time fractional–order logistic model with Allee effect and proportional harvesting. International Journal of Dynamics and Control **11**: 1544–1558.

Panigoro, H. S., A. Suryanto, W. M. Kusumawinahyu, and I. Darti, 2019 Dynamics of a fractional–order predator–prey model with infectious diseases in prey. Communication in Biomathematical Sciences **2**: 1544–1558.

Panigoro, H. S., A. Suryanto, W. M. Kusumawinahyu, and I. Darti, 2021 Dynamics of an eco-epidemic predator–prey model involving fractional derivatives with power-law and Mittag–Leffler kernel. Symmetry **13**: 785.

Petráš, I., 2011 *Fractional–order nonlinear systems: modeling, analysis and simulation*. Springer Science & Business Media.

Rayungsari, M., A. Suryanto, W. M. Kusumawinahyu, and I. Darti, 2022 Dynamical analysis of a predator–prey model incorporating predator cannibalism and refuge. Axioms **11**: 116.

Rayungsari, M., A. Suryanto, W. M. Kusumawinahyu, and I. Darti, 2023 Dynamics analysis of a predator–prey fractional–order model incorporating predator cannibalism and refuge. Frontiers in Applied Mathematics and Statistics **9**: 1122330.

Ruan, M. and X. Li, 2024 Complex dynamical properties and chaos control for a discrete modified leslie–gower prey–predator system with holling ii functional response. Advances in Continuous and Discrete Models **2024**: 30.

Sahoo, K. and B. Sahoo, 2024 Crucial impact of component Allee effect in predator–prey system. Journal of Physics A: Mathematical and Theoretical **57**: 215601.

Santra, P. K. and G. S. Mahapatra, 2020 Dynamical study of discrete–time prey–predator model with constant prey refuge under imprecise biological parameters. Journal of Biological Systems **28**: 681–699.

Sarkar, K. and B. Mondal, 2023 Dynamic analysis of a fractional–order predator–prey model with harvesting. International Journal of Dynamics and Control **11**: 1518–1531.

Selvam, A. G. M., R. Janagaraj, and M. Jacintha, 2020 Dynamical analysis of a discrete fractional order preypredator system incorporating a prey refuge with holling type ii response. In *Journal of Physics: Conference Series*, volume 1597, p. 012008.

Shabbir, M. S. and Q. Din, 2022 Understanding cannibalism dynamics in predator–prey interactions: bifurcations and chaos control strategies. Qualitative Theory of Dynamical Systems **23**.

Suryanto, A., I. Darti, H. S. Panigoro, and A. Kilicman, 2019 A fractional–order predator–prey model with ratio–dependent functional response and linear harvesting. Mathematics **7**: 1100.

Uddin, M. J., P. K. Santra, S. M. S. Rana, and G. S. Mahapatra, 2024 Chaotic dynamics of the fractional order predator–prey model incorporating Gompertz growth on prey with Ivlev functional response. Chaos Theory and Applications **63**: 192–204.

Ulfa, H. M., A. Suryanto, and I. Darti, 2017 Dynamics of Leslie–Gower predator–prey model with additional food for predators. International Journal of Pure and Applied Mathematics **115**: 199–209.

Zhang, H., Y. Cai, S. Fu, and W. Wang, 2019 Impact of the fear effect in a prey–predator model incorporating a prey refuge. Applied Mathematics and Computation **356**: 328–337.

How to cite this article: Suryanto, A., Darti, I., and Cahyono, E. Bifurcation Analysis and Chaos Control of a Discrete-Time Fractional Order Predator-Prey Model with Holling Type II Functional Response and Harvesting. *Chaos Theory and Applications*, 7(1), 87-98, 2025.